Effect of annealing on the structure of an amorphous $(Mo_{0.6}Ru_{0.4})_{82}B_{18}$ alloy

C. C. Koch, D. M. Kroeger, J. S. Lin,* and J. O. Scarbrough
Metals and Ceramics Division, Oak Ridge National Laboratory, Oak Ridge, Tennessee 37830

W. L. Johnson
W. M. Keck Laboratory of Engineering, California Institute of Technology, Pasadena, California 91125

A. C. Anderson
Department of Physics, University of Illinois at Urbana-Champaign, Urbana, Illinois 61801
(Received 13 September 1982)

The amorphous metallic glass $(Mo_{0.6}Ru_{0.4})_{82}B_{18}$ was annealed for various lengths of time at temperatures up to 650 °C. The changes in structure due to these annealing treatments were determined by measurements of superconducting properties (T_c,B_{c2},J_c), electrical resistivity (ρ_n), low-temperature specific heat (electronic coefficient γ), small-angle x-ray scattering (SAXS), and transmission electron microscopy (TEM). At lower annealing temperatures ($\lesssim 450$ °C) only small changes occurred in the composition-dependent parameters (T_c,γ) but large degradations were exhibited in those quantities (J_c, fracture strain) sensitive to the defect structure. No evidence of microstructural changes was revealed by SAXS or TEM in this regime. At higher annealing temperatures (or longer times) evidence for the development of, first, phase separation, then, the beginnings of crystallization was found by SAXS and TEM. In this regime larger degradations of T_c and γ occurred along with a change in the form of the $F_p(b)$ curve (i.e., a change in the fluxoid pinning mechanism). The above observations imply annealing-induced long-range compositional variations. The activation energy for the onset of long-range compositional inhomogeneity was determined to be 309 kJ mol^{-1} (3.2 eV).

I. INTRODUCTION

It has become clear in recent years that some sort of inhomogeneities or structural defects must be influencing many of the properties of metallic glasses. Metallic glasses are obtained by rapid solidification. The liquid state can be "trapped" by cooling down below the glass transition temperature T_g, before nucleation of the crystalline state can occur. During rapid quenching the atoms do not have time to relax to their lower-temperature configuration, and therefore the quenched glass exists in a metastable state with respect to a relaxed, more stable glassy state as well as to the crystalline state. On annealing, the metastable quenched-in structure relaxes to more stable configurations. This structural relaxation is a fundamental characteristic of amorphous alloys. Relaxation phenomena also have been documented for amorphous polymers and oxides. Relaxation in metallic glasses can influence a wide range of physical properties including density as well as magnetic and electrical properties. It has become well established that structural relaxation must be taken into account when studies are made of kinetic processes such as diffusion and viscosity. A microscopic model for structural relaxation in metallic glasses has recently been proposed by Egami, Vitek, and Srolovitz.[1] They review the changes in physical properties that can occur during structural relaxation and present a model based on their description of defects in the amorphous structure.[2,3] They have defined structural defects in terms of atomic-level internal stresses and local symmetry coefficients as determined from a computer-generated model of the amorphous structure. The results of their analysis provide two kinds of defects: (1) positive or negative local-density fluctuations and (2) regions of large shear stress and large deviations from spherical symmetry.

The radial distribution function (RDF) determined from diffraction experiments is the only directly observable structural quantity. Srolovitz *et al.*[3] have compared the RDF from relaxed regions of their computer-generated model with the RDF from the defects. The difference in these RDF's was assumed to simulate an annealing experiment if annealing serves to annihilate defects—mainly by recombination of positive- with negative-density fluctuation regions. The calculated RDF showed a marked similarity to an experimentally

measured change in RDF due to annealing.[4] The experimentally determined RDF had been determined by energy-dispersive x-ray diffraction. This model would appear to account for certain observations like the small change in density ($\sim 0.5\%$) on relaxation[5] better than the older free-volume models.[6,7]

In addition to density fluctuations, metallic glasses have also been observed to undergo phase separation[8–10] into two amorphous phases. Such observations were made by use of small-angle x-ray scattering (SAXS) and transmission electron microscopy (TEM). Phase separation results in an inhomogeneous material on a spatial scale which ranges from nanometers to micrometers and certainly influences physical properties of the material.

More experimental verification of the nature of defects and inhomogeneities in metallic glasses is needed. One approach to this problem is to study a structure-sensitive property as a function of thermal or mechanical treatments which are likely to change the defect density or distribution. We have observed that the superconducting critical current density J_c can be reduced $\sim 50\%$ by inhomogeneous deformation of an amorphous $(Mo_{0.6}Ru_{0.4})_{82}B_{18}$ alloy.[11] J_c is an extremely structure-sensitive property which is controlled by the interaction of the superconducting fluxoid lattice with inhomogeneities (defects). Furthermore, J_c provides some guidance on the "size" of the defect responsible for fluxoid pinning since inhomogeneities much smaller than the superconducting coherence length will not influence J_c. This value is 8.3 nm for $(Mo_{0.6}Ru_{0.4})_{82}B_{18}$.[11] We concluded J_c could be used as a probe of the defect structure in metallic glasses.

Small-angle x-ray or neutron scattering can be used to study inhomogeneities in the range 1.0 to 100.0 nm, precisely the range expected for the size of defects in metallic glasses. Since small-angle x-ray scattering is only sensitive to fluctuations in electron density, it is a probe of inhomogeneities that does not depend on the periodicity of the atomic structure.

This paper reports the results of annealing experiments on the amorphous alloy $(Mo_{0.6}Ru_{0.4})_{82}B_{18}$ in which J_c and SAXS measurements were used as the principal probes of the structural changes. The superconducting transition temperature T_c, and upper critical field B_{c2}, are much less structure-sensitive parameters. However, small changes in T_c have been reported for relaxation in several metallic glasses[12,13] and T_c and B_{c2} were also monitored in this study. The electronic coefficient of low-temperature specific heat was obtained from the superconducting measurements as well as being directly measured by heat capacity. In addition, the fracture strain was determined as a function of annealing whereas high-angle x-ray diffraction and transmission electron microscopy were used to search for evidence of crystallization.

II. EXPERIMENTAL

Amorphous alloys of composition $(Mo_{0.6}Ru_{0.4})_{82}B_{18}$ were prepared in an arc hammer apparatus at Oak Ridge National Laboratory (ORNL) or a two-piston apparatus at California Institute of Technology (Cal. Tech.) as previously described.[14,15] The rapidly quenched foils were typically 1.5 to 2.0 cm in diameter and 30 to 40 μm thick. After quenching, the foils were examined by high-angle x-ray diffraction in Norelco (Cal. Tech.) or Philips (ORNL) diffractometers using Cu $K\alpha$ radiation and step-scanning at 0.1° intervals (Cal. Tech.) or 0.02° intervals (ORNL). The typical amorphous diffraction pattern was observed in all cases. Samples showing any resolvable Bragg peaks, which indicate some crystalline material, were rejected.

Samples for superconducting property measurements were cut from the quenched disks in the shape of strips 8–10-mm by 2 mm wide with a diamond slitting saw. These samples were encapsulated in quartz tubes which had been evacuated to a pressure of 1.3×10^{-5} Pa (1×10^{-7} Torr) and backfilled with a partial pressure of pure argon.

Samples for SAXS and TEM were cut from the foils in the form of 3-mm diam. disks and similarly encapsulated. For many of the SAXS specimens an entire quenched foil was used. The samples for SAXS were thinned either by mechanical polishing on 600-grit emery paper or electrolytically to ~ 10–15 μm (~ 2 optimum transmission thicknesses for Cu $K\alpha$ x radiation). Since samples thinned by both of these techniques exhibited identical results for the same condition it was concluded that the mechanical polishing was not affecting the structure. Annealing was carried out in muffle furnaces. Since deviations in the precise boron concentration and quenched-in defect structure might result in scatter in the superconducting property measurements, the same samples were used for isochronal (1 h) anneals at temperatures up to 600 °C for the J_c measurements. That is, the samples were consecutively annealed, measured, annealed at the next-higher temperature, measured, etc. Samples for the SAXS measurements in which more and longer annealing times were used were taken from the same quenched disk as much as possible for a series of times or temperature.

A standard four-probe resistive method was used to measure J_c. These measurements were made in liquid He at 4.2 K. A voltage criterion of 2 μV was

taken to define J_c. The magnetic field, provided by a 7.2-T superconducting solenoid, was applied perpendicular to the wide surface of the samples to minimize contributions from surface pinning. Normal-state resistivity was also measured from T_c up to room temperature. While T_c measurements were determined resistively, more accurate values were obtained by an ac susceptibility technique which has been described elsewhere.[16] A calibrated Ge thermometer was used as the temperature sensor and a pure lead sample was kept in the measuring coils as an internal calibration check for temperature measurement.

Low-temperature heat capacities C were measured using a small-sample calorimeter of a design similar to that described by Räde[17] and by Stewart and Giorgi.[18] The thermal relaxation method was used with an electronic system roughly similar to that described in Ref. 19. The sample holder used for these measurements consisted of a 1.9-cm diam., 0.025-cm thick sapphire disk on which an amorphous CuZr heater was vapor-deposited. The gold leads of a germanium resistance thermometer (trimmed to a length of 2 mm) were attached to the disk and to 0.004-cm diam. manganin leads with silver-impregnated electrically and thermally conductive epoxy. Heater leads and an 0.005-cm diam. copper wire, approximately 15-cm long and wound into a coil, which served as a heat link between the sample assembly and a heat reservoir, were similarly attached to the disk. Samples were stuck to the disk with 200—400 μg of Apiezon N grease, the heat capacity of which has been measured by others.[20,21] Our sample mass was approximately 20 mg, and its heat capacity was about half of the total for sample plus addenda (sample holder and grease) at 7 K. Thus, our major error is uncertainty in the previously measured heat capacity of the sample holder. A 50-mg, high-purity copper disk, which over the temperature range of interest (6—11 K) has a heat capacity approximately the same as our specimen's, was used as a standard. Several measurements of this standard, with this and other addenda, have yielded values of the intercept γ and the slope β of C/T vs T^2 which were all within 4% of the accepted literature values for copper. For the MoRuB specimens, the individual data points generally deviated from the linear least-squares fit of C/T vs T^2 by less than 3%. The error bars in Fig. 2 represent the 2σ or 95% confidence limits for the value of γ as determined by the scatter in the data.

The small-angle x-ray scattering experiments were performed on the ORNL 10-m small-angle x-ray scattering camera.[22] Cu $K\alpha$ radiation was used. The incident radiation was monochromated by diffraction from the (00.2) planes of a pyrolytic graphite crystal and collimated with two 1×1-mm^2 slits separated by 1.2 m. The scattered radiation was recorded with a two-dimensional position-sensitive x-ray detector and then stored in the memory of a minicomputer. The incident-beam power was calibrated by the multiple-foil method using pure nickel foils. After the background had been subtracted and correction made for the spatial sensitivity of the detector, isointensity contour maps for each specimen were plotted. Based on the isointensity contour maps, the circular averages of the scattering intensity $I(K)$ were computed, where the scattering vector $K=(4\pi/\lambda)\sin\theta$ and 2θ is the scattering angle. We have identified multiple scattering as a significant contribution to the higher-angle ($K>2$ nm^{-1}) scattering intensity. This region of "flat" I vs K, presumably due to a combination of multiple scattering and Laue monotonic intensity terms, was subtracted from the intensity which was normalized to absolute electron units. This corrected intensity was compared to Guinier's law and Porod's law.[23] In those samples which appeared to obey the Guinier and Porod laws a size distribution of the scattering entity was calculated using an analytical method developed by Fedorova and Schmidt[24] and modified by Yoo *et al.*[25]

The strain to fracture in bending E^f was measured on the annealed $(Mo_{0.6}Ru_{0.4})_{82}B_{18}$ samples as an estimate for ductility. This measurement was carried out by bending the foils around progressively smaller diameter cylinders until fracture was observed. The strain was determined by $t/2r$, where t is the sample thickness and r is the radius of curvature at which fracture occurs. Some samples could be folded back on themselves without fracture. The yield strain E^y (0.025) previously determined for this material was used to normalize the data. Thus a sample which did not fracture on folding back on itself but did plastically yield, would have $E^f/E^y=1.0$ since in tension, in a metallic glass $E^f\approx E^y$. Samples exhibiting some embrittlement would thus give values of $E^f/E^y<1.0$.

III. DISCUSSION OF EXPERIMENTAL RESULTS

A. T_c, B_{c2}, ρ_n, and γ

The superconducting transition temperatures T_c were normalized by dividing by the T_c for the as-cast samples T_{c0}. A plot of T_c/T_{c0} vs annealing temperature is presented in Fig. 1 for four different samples. It is apparent that at temperatures of 300 °C or higher T_c shows a degradation from T_{c0}, which is temperature, time, and specimen dependent. The degradation observed was a maximum of about 16% for sample B annealed 500 h at 600 °C.

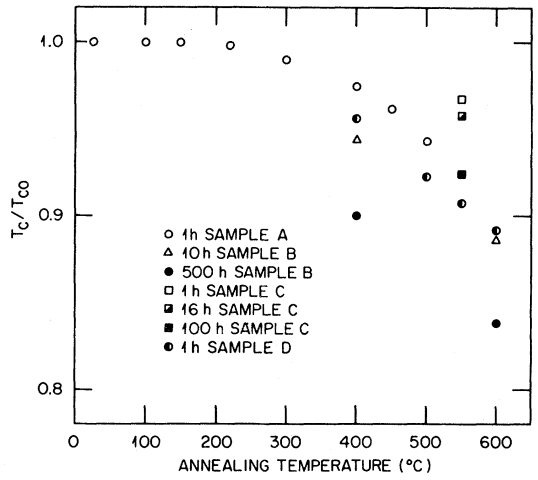

FIG. 1. Normalized superconducting transition temperature T_c/T_{c0} vs annealing temperature.

For sample A, given progressive 1-h anneals, values for B_{c2}, ρ_n (normal-state resistivity), and $dB_{c2}/dT\,|_{T_c}$ were also measured and are listed in Table I. B_{c2} decreases slowly with increasing temperature, reaching a minimum at 450 °C (18% decrease) and then rises dramatically at 500 °C (25% increase). This behavior is also reflected in $dB_{c2}/dT\,|_{T_c}$, which first decreases (11%) up to 400 °C then increases again at 500 °C by ~27%. Values for ρ_n exhibit changes of less than 5% over the range of annealing temperatures, which is probably within the limits of experimental error for this measurement. The Sommerfeld constant γ can be calculated from the above parameters according to the Ginzburg-Landau-Abrikosov-Gor'kov (GLAG) theory for type-II superconductors by the expression

$$\gamma = -\frac{\pi^3}{12}\frac{k_B}{e}\frac{1}{\rho_n}\frac{dB_{c2}}{dT}\bigg|_{T_c}, \tag{1}$$

TABLE I. Superconducting parameters used in calculating γ.

Annealing temperature (°C)	B_{c2} (T)	ρ_n (Ω m)	$dB_{c2/dT}$ (T/K)	γ (mJ/mol K^2)
25	5.65	1.48×10^{-6}	2.35	2.87
100	5.65	1.48×10^{-6}	2.35	2.87
150	5.55	1.49×10^{-6}	2.31	2.80
220	5.35	1.46×10^{-6}	2.24	2.77
300	5.25	1.49×10^{-6}	2.24	2.72
400	4.70	1.53×10^{-6}	2.10	2.48
450	4.65	1.50×10^{-6}	2.16	2.60
500	5.80	1.55×10^{-6}	2.86	3.33

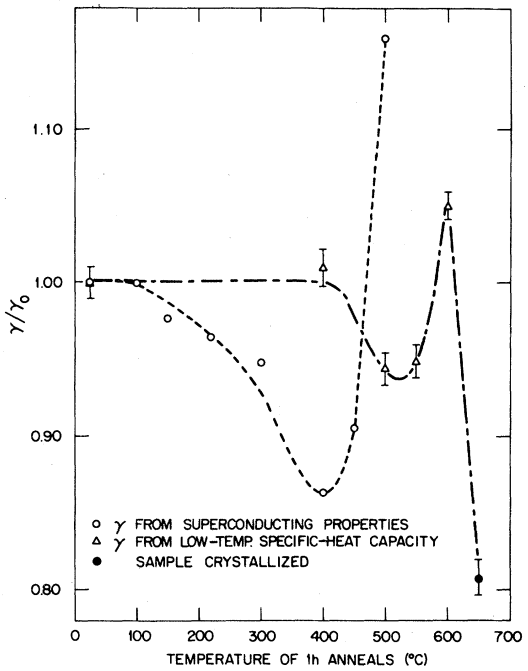

FIG. 2. Normalized electronic coefficient of low-temperature specific-heat capacity γ/γ_0 vs annealing temperature for 1-h anneals.

where k_B is the Boltzmann constant and e is the electron charge. This expression should be applicable near T_c and in the dirty limit, that is, where the normal electron mean free path is much less than the superconducting coherence length. This criterion is met by $(Mo_{0.6}Ru_{0.4})_{82}B_{18}$ since the coherence length is 8.3 nm (at 4.2 K) and the mean free path is ~0.3–0.4 nm.[11] It has been shown that γ calculated from the GLAG expression agrees closely with γ determined from low-temperature specific-heat capacity measurements for $(Mo_{0.6}Ru_{0.4})_{100-x}B_x$ alloys.[26]

The T_c/T_{c0} values for sample D in Fig. 1 were obtained from the low-temperature specific-heat capacity measurements. Sample D apparently shows a slightly greater degradation in T_c at a given annealing temperature than sample A for progressive 1-h anneals.

The variation of γ with annealing temperature as calculated from the GLAG theory is also given in Table I for sample A. The values of γ normalized by γ_0, the value for the as-cast samples, are plotted against annealing temperature in Fig. 2 for sample A (γ calculated from the GLAG theory), and sample D (γ obtained from low-temperature specific-heat capacity measurements). The γ_0's for these samples differed by $<5\%$; sample A, $\gamma_0=2.87$ mJ/mol K^2, sample D, $\gamma_0=3.01$ mJ/mol K^2. Both samples first exhibit a decrease with increasing annealing tem-

perature followed by a sharp increase to γ values greater than γ_0. Sample *D* showed a further marked decrease after annealing at 650 °C, a heat treatment which produced partial crystallization as revealed by x-ray diffraction. The structure of samples *A* and *D* for all lower annealing temperatures in Fig. 2 was amorphous to the resolution of high-angle x-ray diffraction, and confirmed by the results of SAXS and TEM to be described below. Since γ is proportional to the density of electronic states at the Fermi level $N(E_F)$, the electronic structure of amorphous $(Mo_{0.6}Ru_{0.4})_{82}B_{18}$ undergoes substantial changes on annealing in the temperature range 400–600 °C. The Debye temperature Θ_D, measured for sample *D* of 320 K, showed a small increase for annealing temperatures >400 °C to ~ 340 K and remained essentially constant at the higher-temperature anneals.

The differences in the γ vs annealing temperature behavior between samples *A* and *D* suggest different kinetics for the structural and/or compositional changes responsible. That is, sample *A* would appear to have enhanced kinetics due to, perhaps, differences in the quenched-in glassy structure, compositional variations, etc. However, the degradation of T_c on annealing is comparable for the two samples (Fig. 1) with a slightly faster decrease for sample *D*. A possible explanation for these contradictory results may reside in the measuring techniques. Low-temperature specific-heat capacity is a bulk property measurement, whereas dB_{c2}/dT depends on the connectivity of the material, i.e., a continuous filament with a lower value for B_{c2} can mask the higher B_{c2} of its matrix. If this explanation for the results shown in Fig. 2 should be correct, it implies that the amorphous $(Mo_{0.6}Ru_{0.4})_{82}B_{18}$ alloys become compositionally inhomogeneous during annealing at the higher temperatures. Evidence for the development on annealing of compositional inhomogeneity will be presented for the other experimental probes to be discussed.

B. J_c, F_p

The bulk pinning force F_p was calculated from the experimental values for J_c and B ($F_p = BJ_c$). In Fig. 3, F_p is plotted against the reduced field $b = B/B_{c2}$. The solid curve represents the $F_p(b)$ values for as-cast amorphous $(Mo_{0.6}Ru_{0.4})_{82}B_{18}$. This sample was annealed at progressively higher temperatures. As illustrated in Fig. 3, annealing at temperatures up to 450 °C results in the degradation of F_p. The shape of the F_p-vs-b curve stays the same with the maximum in F_p remaining at about $b = 0.15$. This degradation in F_p is very similar to that which we have observed after inhomogeneous deformation of amorphous $(Mo_{0.6}Ru_{0.4})_{82}B_{18}$ (Ref. 11). The degradation increases with increasing annealing temperature up to 450 °C. At this temperature the lower-field portion ($b \leq 0.5$) of the F_p-vs-b curve continues to be degraded while an increase in F_p is observed for $b > 0.5$. After the 500 °C anneal the shape of the F_p-vs-b curve has been completely altered with the maximum in F_p occurring near $b = 0.4$. The change in shape of the F_p (b) curves and the increase in the magnitude of F_p for the 500 °C anneal suggest that a different fluxoid pinning mechanism is activated at the higher annealing temperatures (≥ 450 °C). The changes in F_p with annealing temperature are illustrated explicitly in Fig. 4 by normalizing F_p by F_p for the as-cast condition for two values of reduced field; $b = 0.15$ which represents the peak in F_p for the as-cast condition and annealing temperature ≤ 450 °C, and $b = 0.5$. F_p/F_p as-cast is seen to decrease with annealing temperature to a minimum at 400 °C where a degradation of 55–60 % is noted. That F_p (J_c) is a sensitive parameter to monitor structural changes can be illustrated by comparing Fig. 4 with Fig. 1. A 1-h anneal at 300 °C produces only a 1% change in

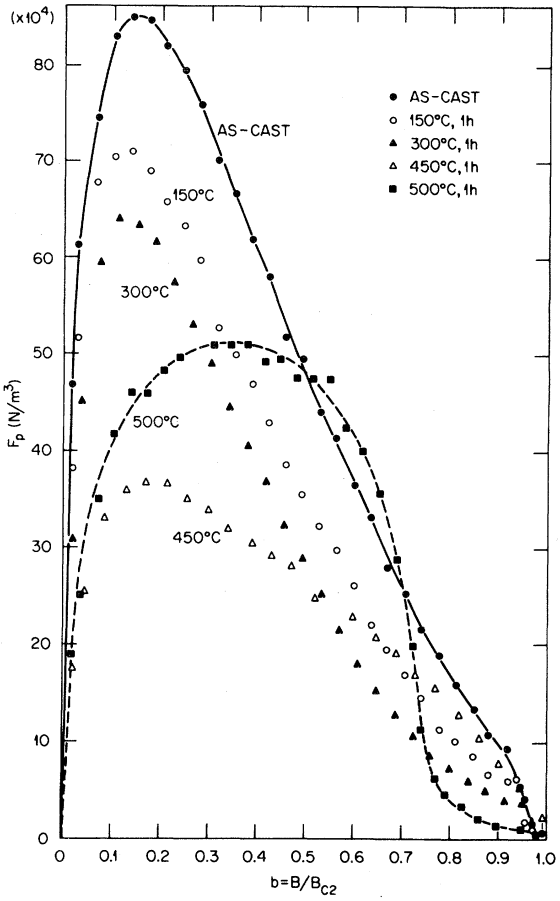

FIG. 3. Volume fluxoid pinning force F_p vs reduced field $b = B/B_{c2}$.

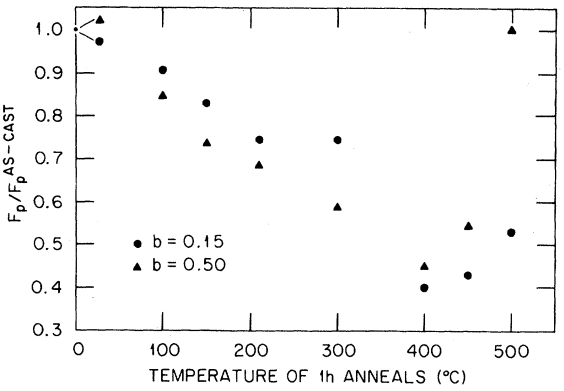

FIG. 4. Normalized volume pinning force $F_p/F_p^{\text{as-cast}}$ vs annealing temperature for 1-h anneals.

T_c/T_{c0} (Fig. 1) while the same treatment changes F_p (J_c) by 25—40% (depending on the b chosen). It would appear that the short-range changes in topological and chemical order which occur during relaxation of the as-cast structure ($T_a \leq 450$ °C) have only a small effect on T_c, which is mainly controlled by composition, while F_p (J_c), which is sensitive to inhomogeneities on the scale (or larger) of the superconducting coherence distance (8.3 nm), shows substantial changes. The larger effects observed in T_c and γ at annealing temperatures ≥ 450 °C along with the apparent drastic change in fluxoid pinning mechanism imply a substantial alteration of the structure of amorphous $(Mo_{0.6}Ru_{0.4})_{82}B_{18}$. The SAXS results presented in the next section were performed to help understand these changes.

C. SAXS

The SAXS measurements were carried out on a series of $(Mo_{0.6}Ru_{0.4})_{82}B_{18}$ samples annealed for a wider range of times and temperatures than had been used in the study of J_c. Figure 5 presents a SAXS data set for a sample annealed 315 h at 550 °C. The intensity, corrected for background, etc. but given in arbitrary units, is plotted against $K=4\pi\sin\theta/\lambda$ where $\lambda=0.154$ nm for copper $K\alpha$ radiation. The "flat" portion of the $I(K)$ curve for $2 \leq K \leq 3.5$ nm^{-1} is believed to be due to a combination of multiple scattering and the Laue monotonic contribution. This intensity was thus subtracted from the intensity for $K<2$ nm^{-1} to isolate the scattering from the inhomogeneities of interest. After this was done and the intensity data put into absolute (electron) units, plots of ln$I$ vs K were made. In Fig. 6 we illustrate four curves which are representative of the SAXS data observed. Curve

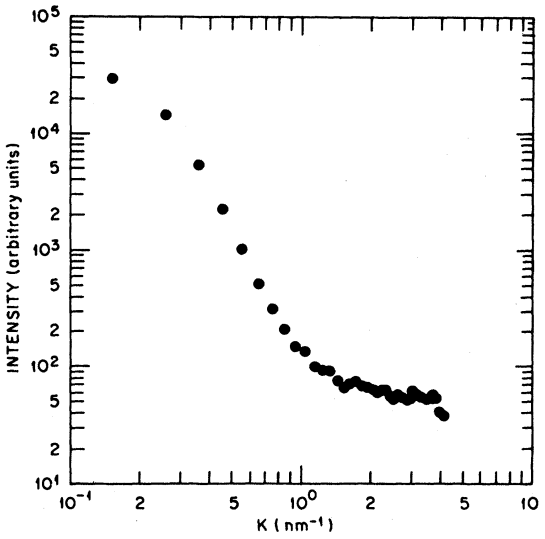

FIG. 5. SAXS intensity vs $K=4\pi\sin\theta/\lambda$ for amorphous $(Mo_{0.6}Ru_{0.4})_{82}B_{18}$ annealed 315 h at 550 °C.

"A" is for a sample in the as-cast condition. The SAXS intensity is relatively low, and attempts to fit the data to either Guinier's or Porod's law were unsuccessful. Samples annealed at low temperatures (<450 °C) showed no measurable changes in the SAXS data from that of the as-cast condition. (Al-

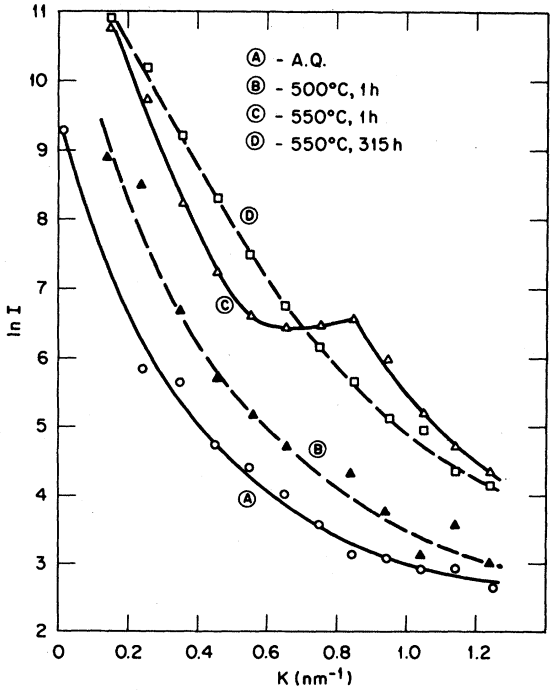

FIG. 6. ln of SAXS intensity (absolute units) vs $K=4\pi\sin\theta/\lambda$.

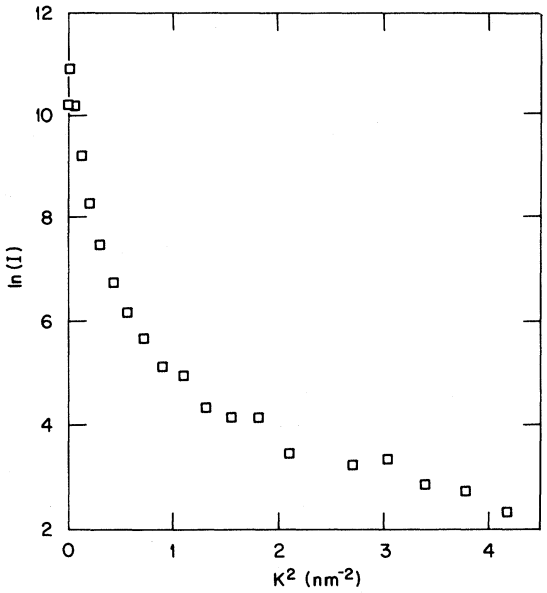

FIG. 7. ln of SAXS intensity (absolute units) vs K^2. Guinier plot, the slope of ln$I$ vs K^2 at $K^2=0$ provides the radius of gyration of the scatterer by slope $=-R_G^2/3$.

though there is considerable scatter in the data, there is an indication that the SAXS intensity may even have decreased under these annealing conditions.) At somewhat higher annealing temperatures, behavior as shown by curve "*B*" is observed, which is for a sample aged 1 h at 500 °C. The SAXS intensity is increased over that for the as-cast condition, but the Guinier or Porod laws are still not able to fit the data. At still higher annealing temperatures or

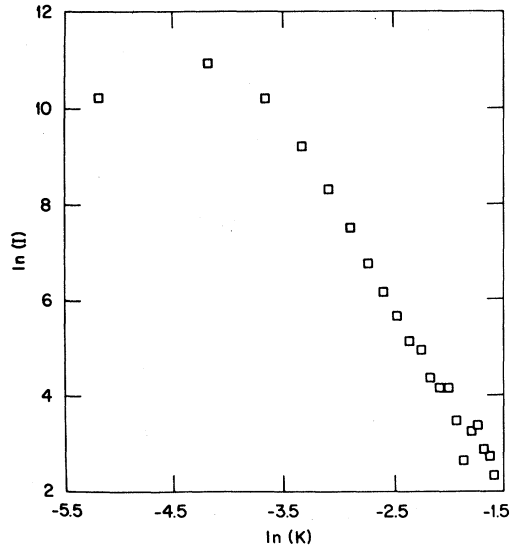

FIG. 8. ln of SAXS intensity (absolute units) vs ln of K. Porod plot. Slope of four indicates Porod's law is obeyed.

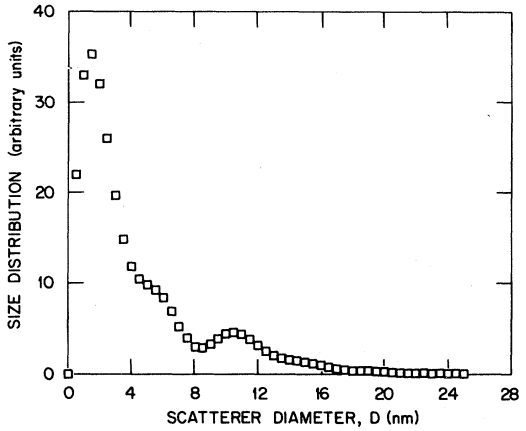

FIG. 9. Size distribution of scatterers. Size distribution vs scatterer diameter.

longer times, peaks in the $I(K)$ curves are observed as illustrated by curve "*C*" for a sample aged 1 h at 550 °C. Peaks in $I(K)$ such as this are not readily explained by the theory of small-angle scattering. They can be assumed to represent a "pseudo-Bragg peak" attributed to a periodicity in the scattering entity. If this assumption is made, the $I(K)$ peak for curve C would represent a periodicity of $\sim$7.9 nm. After still higher annealing temperatures or longer times, the peaks in $I(K)$ disappear and curves such as "*D*" are obtained. The data of curve D can now be fitted to the Guinier law and the Porod law as illustrated in Figs. 7 and 8, respectively. The radius of gyration for the scatters calculated from the fit to Guinier's law[23] is 6.8 nm while that determined from Porod's law[23] is 5.5 nm. The distribution of the size of the scatterers versus the diameter of the scatterers, if spherical entities are assumed, is presented in Fig. 9. A distribution of size with

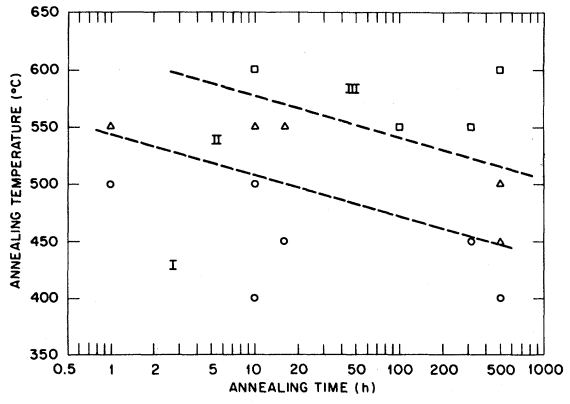

FIG. 10. Annealing temperature vs $\log_{10}$ annealing time. Region I: SAXS comparable to as-cast samples; Guinier or Porod laws not obeyed. Region II: Peaks in I vs K curves—periodic scattering entities. Region III: Guinier and Porod laws obeyed, discrete scatterers.

peaks at ~2.0, 5.0, and 11.0 nm is observed. The average diameter of this distribution is 4.3 nm.

The SAXS results are summarized by the annealing temperature vs $\log_{10}$ time plot of Fig. 10. The data can be separated into three regions. In region I represented by circular data points, little difference is observed in the scattering intensity from that of the as-cast condition. No Guinier or Porod region is seen. In region II, with triangular data points, peaks in the $I(K)$ curve are noted as in curve C of Fig. 6 but the data do not fit either the Guinier or Porod laws. Finally, at the highest temperatures and longest annealing times, region III represented by the square data points gives $I(K)$ curves which can be fitted by Guinier's and Porod's laws. While none of the samples represented in Fig. 10 showed any evidence for crystallization to the resolution of high-angle x-ray diffraction, transmission electron microscopy revealed small (5—10 nm) crystalline precipitates present in region III where Guinier's and Porod's laws are obeyed, but not in the other regions.

The boundary between region I and II (Fig. 10) is well defined. Therefore, an activation energy could be determined for the rate of the development of the periodic entities in region II. Aging time versus $1/T$ is presented in Fig. 11 for this boundary, providing an activation energy of 309 kJ mol^{-1} (3.2 eV). This value for an activation energy falls within the range of activation energies observed for crystallization in several metallic glass systems.[27]

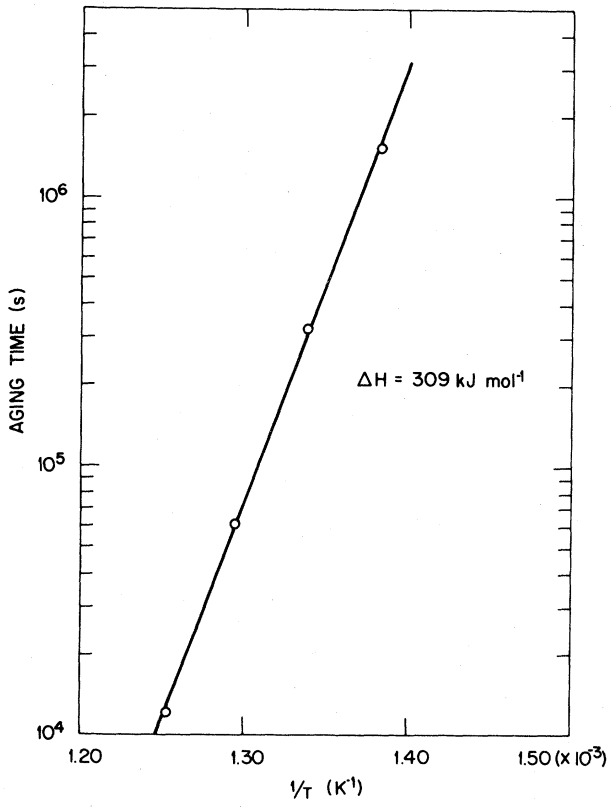

FIG. 11. $\log_{10}$ annealing time vs reciprocal of absolute annealing temperature for the onset of region II, Fig. 10.

D. Fracture strain

The strain to fracture E^f, normalized by the yield strain $E^y=0.025$, is plotted against annealing temperature in Fig. 12. In samples which yield plastically E^f/E^y is defined to be equal to 1. It is clear that annealing causes embrittlement of amorphous $(Mo_{0.6}Ru_{0.4})_{82}B_{18}$ which is both temperature and time dependent—that is, a kinetic phenomenon. There is no obvious correlation between the SAXS results and the onset of embrittlement. Embrittlement begins in region I of Fig. 10 where no clear change in SAXS is evident. For example, the specimen aged 1 h at 500 °C exhibits no embrittlement while the sample annealed 10 h at 500 °C shows considerable embrittlement even though their SAXS curves are very similar. Thus the embrittlement observed in $(Mo_{0.6}Ru_{0.4})_{82}B_{18}$ is most probably due to a short-range change in chemical and/or topological order which is not directly observed by SAXS.

IV. DISCUSSIONS

A. Annealing at temperatures <450 °C

The annealing of $(Mo_{0.6}Ru_{0.4})_{82}B_{18}$ at temperatures below 450 °C appears to give rise to structural relaxation similar to that which has been studied in many metallic glasses. The degradation of J_c sug-

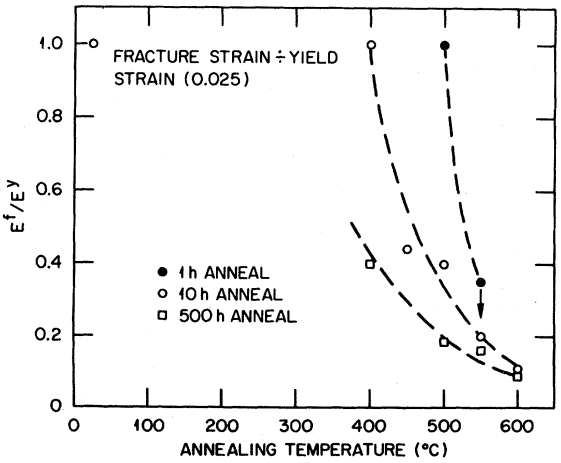

FIG. 12. Fracture strain E^f normalized by the yield strain E^y vs annealing temperature.

gests the annealing of defects responsible for fluxoid pinning. While the nature of the defects existing in metallic glasses is not yet well defined, computer modeling studies[1–3] have recently suggested forms for defects which we can use in our speculation. The positive- and negative-density fluctuations, which are regions of hydrostatic stress, could anneal out by annihilation. While these defects, as modeled, are too small ($\sim$ a few atomic distances) in extent to account for fluxoid pinning in the as-cast structure if randomly distributed, clusters of the defects could provide fluxoid pinning. It is clear that some defect essentially invisible to TEM and SAXS is responsible for the fluxoid pinning and the stress fields of such clusters of density fluctuations might be likely pinning centers. The previous results[11] on degradation of fluxoid pinning by inhomogeneous deformation might also be explained by these defects if mechanical annihilation of the density-fluctuation defects could be assumed.

The small changes in T_c and γ during the relaxation anneals are consistent with previous studies[16,28] and must reflect the short-range atomic movements occurring during relaxation.

The annealing embrittlement of $(Mo_{0.6}Ru_{0.4})_{82}B_{18}$ begins in the temperature-time regime (region I, Fig. 10) in which there is no evidence from SAXS for phase separation. While phase separation has been suggested as the mechanism for annealing embrittlement in several metallic glasses,[29–31] it does not appear responsible for the embrittlement of $(Mo_{0.6}Ru_{0.4})_{82}B_{18}$. Presumably the structural relaxation that occurs in region I and is responsible for the degradation in J_c, causes embrittlement by a short-range change in the topological and/or chemical structure of the alloy.

B. Annealing at temperatures ≥ 450 °C

The changes in the $F_p(b)$ curve, large changes in T_c, γ, and SAXS all suggest a substantial change in the structure of amorphous $(Mo_{0.6}Ru_{0.4})_{82}B_{18}$ which transcends the short-range structural relaxation. The SAXS data point to the development of periodically arranged scatterers (region II, Fig. 10) which then sharpen in extent such that clearly defined "particles" with defined radii of gyration can be inferred from Guinier's and Porod's laws (region III, Fig. 10). Such scatterers might be incipient crystallites. There is no evidence from high-angle x-ray diffraction for crystallization. However, high-resolution transmission electron microscopy and diffraction revealed fine crystalline precipitates in region III, Fig. 10, with diameters of 5–10 nm—consistent with the radii of gyration obtained in the SAXS measurements. Thus, although crystalline phase nucleation does seem to occur ultimately, it occurs only in the latest stages of annealing studied here. No evidence for crystallization could be obtained by TEM for samples in region II. The development of a chemical inhomogeneity without evidence for crystallization suggests phase separation. Piller and Haasen[30] have recently observed the presence of boron-rich domains in the metallic glass $Fe_{40}Ni_{40}B_{20}$ using a novel atom-microprobe technique. Upon annealing their samples well below the glass transition, they observed that these domains grow in spatial extent as well as in boron content. The domains were found to have a typical dimension of 3–5 nm and a boron content of $\sim$25 at.%. The present results on $(Mo_{0.6}Ru_{0.4})_{82}B_{18}$ are consistent with a similar type of microscopic phase separation. Recent studies of $(Mo_{0.6}Ru_{0.4})_{1-x}B_x$ glasses as a function of boron content (x) have suggested that the structure and properties of these glasses change rather rapidly with increasing boron content.[32] This has been interpreted to indicate that alloys with low boron content ($x<0.18$) have predominantly one type of local structure while those with high boron content ($x>0.18$) have a second distinct type of local structure. At $x=0.18$, the glass would seem to contain regions with both types of local structures. The present data suggest that this may result in a phase-separated morphology which grows on annealing at temperatures sufficiently high to permit boron diffusion over atomic scale distances. The growth of these domains could explain the change in the flux pinning profile (Fig. 3) following annealing at temperatures above 450 °C. It could also account for the dramatic increase in small-angle scattering observed after high-temperature annealing, but prior to crystallization.

V. SUMMARY

The changes in structure of the metallic glass $(Mo_{0.6}Ru_{0.4})_{82}B_{18}$ on annealing were followed by several experimental methods. These included measurements of T_c, ρ_n, B_{c2}, γ, J_c, SAXS , TEM, and fracture strain. At lower annealing temperatures (≤ 450 °C) only small changes occurred in the strongly composition-dependent parameters (T_c,γ) while those quantities sensitive to the defect structure (J_c, fracture strain) exhibited substantial degradations. No evidence of structural change was revealed by SAXS or TEM in this regime suggesting short-range atomic rearrangements are responsible for the relaxation processes influencing J_c and fracture strain.

At higher annealing temperatures and longer annealing times evidence for the development of, first, phase separation, then ultimately the beginnings of

crystallization was obtained by SAXS and TEM. These changes, involving longer-range compositional variations, produced larger degradations of T_c and γ and a change in form of the $F_p(b)$ curve, representing a change in the fluxoid pinning mechanism.

The activation energy for the onset of compositional inhomogeneity (and crystallization) was found to be 309 kJ mol^{-1} (3.2 eV) consistent with the range of values obtained by others for crystallization of several metallic glasses.

ACKNOWLEDGMENTS

The authors wish to thank O. B. Cavin for high-angle x-ray diffraction measurements and E. H. Lee for transmission electron microscopy. We also wish to thank A. DasGupta and J. H. Schneibel for reviewing the manuscript. This research was sponsored by the Division of Materials Sciences, U. S. Department of Energy, under Contract No. W-7405-eng-26 with the Union Carbide Corporation.

---

*Present address: Solid State Division, ORNL.

[1]T. Egami, V. Vitek, and D. Srolovitz, *Proceedings of the 4th International Conference on Rapidly Quenched Metals,* edited by T. Masumoto and K. Suzuki (The Japan Institute of Metals, Sendai, 1982), Vol. 2, p. 517.

[2]T. Egami, K. Maeda, and V. Vitek, Philos. Mag. 41A, 883 (1980).

[3]D. Srolovitz, K. Maeda, V. Vitek, and T. Egami, Philos. Mag. 44A, 847 (1981).

[4]T. Egami, J. Mater. Sci. 13, 2587 (1978).

[5]H. S. Chen, J. Appl. Phys. 49, 3289 (1978).

[6]F. Spaepen, Acta Metall. 25, 407 (1977).

[7]P. Ramachandrarao, B. Cantor, and R. W. Cahn, J. Mater. Sci. 12, 2988 (1977).

[8]C. P. Chen and D. Turnbull, J. Non-Cryst. Solids 17, 169 (1975).

[9]L. Tanner and R. Ray, Scr. Metall. 14, 657 (1980).

[10]C. O. Kim and W. L. Johnson, Phys. Rev. B 23, 143 (1981).

[11]C. C. Koch, J. O. Scarbrough, and D. M. Kroeger, *Proceedings of the 4th International Conference on Rapidly Quenched Metals,* edited by T. Masumoto and K. Suzuki (The Japan Institute of Metals, Sendai, 1982), Vol. 2, p. 1229; C. C. Koch, J. O. Scarbrough, D. M. Kroeger, and A. DasGupta, Appl. Phys. Lett. 37, 451 (1980).

[12]A. J. Drehman and W. L. Johnson, Phys. Status Solidi A 52, 499 (1979).

[13]P. Esquinazi, M. E. de la Cruz, and F. de la Cruz, Physica 108B, 1215 (1981).

[14]D. M. Kroeger, W. A. Coghlan, D. S. Easton, C. C. Koch, and J. O. Scarbrough, J. Appl. Phys. 53, 1445 (1982).

[15]P. Duwez, *Progress in Solid State Chemistry 3,* edited by H. Reiss (Pergamon, Oxford, 1966).

[16]A. C. Anderson, C. C. Koch, and J. O. Scarbrough, Phys. Rev. B 26, 1156 (1982).

[17]H. S. Räde, Feinwerktechnik Messtechnik 83, 230 (1975).

[18]G. R. Stewart and A. L. Giorgi, Phys. Rev. B 17, 3534 (1978).

[19]R. E. Schwall, R. E. Howard, and G. R. Stewart, Rev. Sci. Instrum. 46, 1054 (1975).

[20]A. J. Bevolo, Cryogenics 14, 661 (1974).

[21]M. Wun and N. E. Phillips, Cryogenics 15, 36 (1975).

[22]R. W. Hendricks, J. Appl. Crystallogr. 11, 15 (1978).

[23]A. Guinier and G. Fournet, *Small Angle Scattering of X-Rays* (Wiley, New York, 1955).

[24]I. S. Fedorova and P. W. Schmidt, J. Appl. Crystallogr. 11, 405 (1978).

[25]M. H. Yoo, J. C. Ogle, B. S. Borie, E. H. Lee, and R. W. Hendricks, Acta Metall. 30, 1733 (1982).

[26]W. L. Johnson, J. Phys. 41, C8-731 (1980).

[27]H. S. Chen and K. A. Jackson, *Ultra Rapid Quenching of Liquid Alloys,* Vol. 20 of *Treatise on Materials Science and Technology,* edited by Herbert Herman (Academic, New York, 1981), p. 241.

[28]A. Ravex, J. C. Lasjaunias, and O. Bethoux, Physica 107B, 397 (1981).

[29]H. S. Chen, Mat. Sci. Eng. 26, 79 (1976).

[30]R. Yokota, K. Matusita, Y. Shiraishi, M. Yoshida, and T. Komatsu, *Proceedings of the 4th International Conference on Rapidly Quenched Metals,* edited by T. Masumoto and K. Suzuki (The Japan Institute of Metals, Sendai, 1982), Vol. 2, p. 1357.

[31]J. Piller and P. Haasen, Acta Metall. 30, 1 (1982).

[32]S. Hopkins and W. L. Johnson, Solid State Commun. (in press); W. L. Johnson and A. R. Williams, Phys. Rev. B 20, 1640 (1979).